materials

MDPI

Article

Structure and Properties of Single-Layer MoS_2 for Nano-Photoelectric Devices

Jiaying Jian [1], Honglong Chang [1,*] and Tao Xu [2]

[1] School of Mechanical Engineering, Northwestern Polytechnical University, Xi'an 710072, China; jianjiaying@mail.nwpu.edu.cn

[2] School of Materials Science and Chemical Engineering, Xi'an Technological University, Xi'an 710021, China; xutaobuaa@163.com

* Correspondence: changhl@nwpu.edu.cn; Tel.: +86-029-88492841

Received: 9 December 2018; Accepted: 2 January 2019; Published: 9 January 2019

Abstract: To meet the need for preparing high-performance nano-optoelectronic devices based on single-layer MoS_2, the effects of the heating method (one-step or two-step heating) and the temperature of the MoO_3 source on the morphology, size, structure, and layers of an MoS_2 crystal grown on a sapphire substrate using chemical vapor deposition are studied in this paper. The results show that MoS_2 prepared by two-step heating (the heating of the S source starts when the temperature of the MoO_3 source rises to 837 K) is superior over that of one-step heating (MoO_3 and S are heated at the same time). One-step heating tends to form a mixture of MoO_2 and MoS_2. Neither too low nor too high of a heating temperature of MoO_3 source is conducive to the formation of MoS_2. When the temperature of MoO_3 source is in the range of 1073 K to 1098 K, the size of MoS_2 increases with the rise in temperature. A uniform large-sized triangle with a side length of 100 μm is obtained when the heating temperature of MoO_3 is 1098 K. The triangular MoS_2 crystals grown by the two-step heating method have a single-layer structure.

Keywords: single-layer MoS_2; chemical vapor deposition; heating method; heating temperature

1. Introduction

As the first two-dimensional material discovered, graphene has shown excellent performance in electrical, optical, thermal, and mechanical aspects [1–5]. However, graphene is a semiconductor without a bandgap, which limits its development in optoelectronic devices. Unlike graphene, bulk, multi-layer, and single-layer MoS_2 materials have bandgaps [6]. Bulk MoS_2 is a semiconductor with an indirect bandgap of 1.2 eV. When the thickness of a MoS_2 film reaches the single-layer level, the bandgap will eventually increase by at least 0.6 eV, due to the two-dimensional confinement effect. The reduction in thickness eventually causes the bandgap of the single-layer MoS_2 film to change from an indirect bandgap to a direct one. This change in bandgap results in photoluminescence of high brightness in single-layer MoS_2 [7]. In addition, single-layer MoS_2 has prominent electrical performance, and the transport calculation of the nonequilibrium Green's function shows that the switching ratio of MoS_2 can reach up to 10^{10} [8]. Due to the superior electrical and optical performance of single-layer MoS_2, it has potential application value in the electronic devices and photoelectronic fields [9–13].

MoS_2 has a hexagonal layered crystal structure. A single-layer MoS_2 is composed of three atomic layers, wherein the upper and lower layers are hexagonal planes composed of sulfur atoms, and the middle metal molybdenum atom layer separates the two layers of sulfur atoms. The common preparation methods for single-layer MoS_2 include micromechanical exfoliated, intercalation of lithium ions, liquid phase ultrasonography, and the chemical vapor deposition method [14–17].

The micromechanical exfoliated method is simple and quick, and the exfoliated product is mostly single-layer MoS_2 with high carrier mobility. Its disadvantages are that the number of exfoliated layers cannot be controlled, and industrial production is hard to realize. The intercalation of lithium ions method can prepare high-quality single-layer MoS_2 materials through controlling the lithium ion insertion and exfoliated process by an electrochemical lithium battery device, which has the advantages of large size and high quality, but with a complicated operation process, high equipment requirements, and low exfoliated efficiency. The liquid phase ultrasonography method can prepare a single-layer MoS_2 nanosheet. Since this method is not sensitive to water and air, it is suitable for mass production, and the obtained sheet can be easily assembled into a film. However, it is difficult to control its exfoliated degree, leaving a low concentration of the nanosheet solution after cleavage. Its disadvantage is that the ultrasonic power has great influence on the formation of the nanosheet.

The chemical vapor deposition (CVD) method uses sulfur vapor to chemically react with molybdenum oxide vapor to form MoS_2 [18,19]. The single-layer MoS_2 prepared by this method has excellent optical and electrical performance, and can be applied to devices like new-type resonators and transistors based on two-dimensional materials [20,21]. With a simple preparation process, the CVD method can control the structure, morphology, and size of the MoS_2 film by controlling the reaction temperature, time, and gas flow rate. Single-layer MoS_2 films with a size of 20 to 80 μm have been grown by CVD. However, whether larger-sized single-layer MoS_2 films can be prepared by CVD remains unsolved.

In this paper, the effects of heating methods (one-step and two-step heating) and heating temperature of the MoO_3 source on the morphology, size, structure, and layer number of MoS_2 grown on a sapphire substrate by sulfurized MoO_3 via the CVD method are investigated.

2. Materials and Methods

2.1. Preparation of MoS_2 Film

2.1.1. Treatment of the Sapphire Substrate

A sapphire plate was chosen as the substrate to prepare an MoS_2 crystal by vapor deposition. The sapphire substrate was cleaned in a clean room before the growth experiment. The cleaning of the sapphire plate includes two steps: the substrate was first sonicated in acetone, ethanol, and deionized water for 10 min, respectively, and then was dried with a nitrogen gas gun.

2.1.2. Growth of MoS_2 by Vapor Deposition

A chemical vapor deposition double temperature tube furnace, as shown in Figure 1, was adopted as the growth device for MoS_2. In the experiment, the S powder was first placed in the low temperature zone on the left side of the tube furnace tube, the MoO_3 powder was placed in the high temperature zone in the middle of the furnace tube, and the sapphire substrate was placed flat on the right side of the furnace tube. The purities of the S powder and MoO_3 powder were 99.5%. The sulfur source in the low temperature zone was 15 cm away from the molybdenum source in the high temperature zone, and the molybdenum source was 5 cm away from the sapphire substrate.

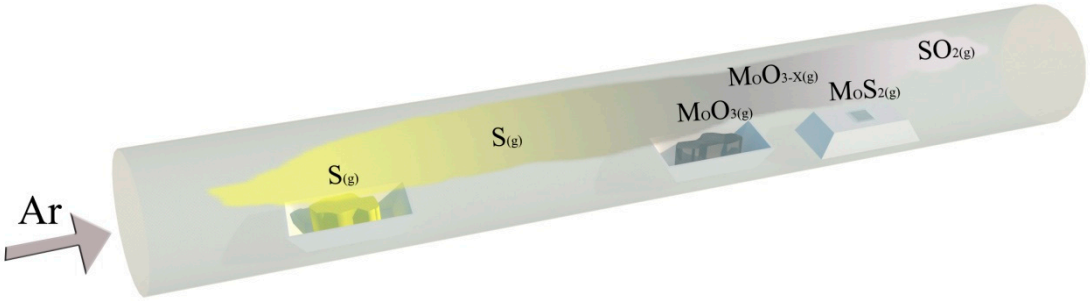

Figure 1. Schematic of the preparation of MoS_2 by chemical vapor deposition (CVD).

After the tube furnace was vacuumed to 10 Torr with a mechanical pump, it was filled with high-purity argon gas at a flow rate of 70 sccm for 30 min. The evacuation–fill processes were repeated three times to vent the air and impurities in the tube furnace. After that, high-purity argon gas was introduced into the tube furnace, and when the pressure reached 1.2 atm, the exhaust valve was opened and adjusted to make the pressure in the furnace greater than 1 atm. Then, the furnace was heated to a setting temperature and held for a certain time. In the heating process, argon gas was continuously introduced into the double temperature tube furnace at a rate of 70 sccm. As a shielding gas, argon gas was also the medium to transmit the sulfur vapor from the low temperature zone to the high temperature zone. At a high temperature, the molybdenum oxide vapor was reduced by the sulfur vapor. The produced gas compound further reacted with sulfur vapor to generate MoS_2, which was deposited onto the sapphire substrate to form MoS_2 crystal. Since the gas volume in the tube furnace shrank with the temperature decrease during the cooling process, which decreased the pressure inside the tube, argon gas was continuously supplied until the temperature was completely lowered to room temperature to prevent outside air from entering the tube furnace.

2.2. Characterization and Test Methods

An SEM (scanning electron microscope; FEI-QUANTA-400, Thermo Fisher, Hillsboro, OR, USA) was used to observe the morphology of the crystal sample grown by chemical vapor deposition. The acceleration voltage of the SEM was 20 kV. For the sample grown by chemical vapor deposition, its morphology can be directly observed by the SEM. The layer number of MoS_2 was roughly judged according to the contrast of color between MoS_2 and the substrate.

The layer number of MoS_2 was determined by Raman spectroscopy (Wissenschaftliche Instrumente und Technologie GmbH, Ulm, Germany) (Renishaw-UK, with a light-passing efficiency of more than 30%, a spectral range of 200 to 1000 nm, a spectral resolution of 1 cm^{-1}, and a spatial resolution of 0.5 μm in the lateral direction and 2 μm in the longitudinal direction) and a homemade photoluminescence spectrometer. The wavelength of Raman spectroscopy was 532 nm, and its grating groove density was 1800 L/mm. The wavelength of photoluminescence spectrometer was 700 nm, and its groove density was 150 L/mm.

3. Results and Discussion

3.1. Effect of Heating Method on the Morphology and Layer Number of MoS_2 Crystals

The effects of the heating method (one-step and two-step heating) on the morphology and layer number of MoS_2 crystals were investigated. The temperature-increase curve of one-step heating is shown in Figure 2a. In this experiment, the high temperature zone (MoO_3) and the low temperature zone (S) were heated simultaneously at two constant rates, and they reached the set temperatures at the same time.

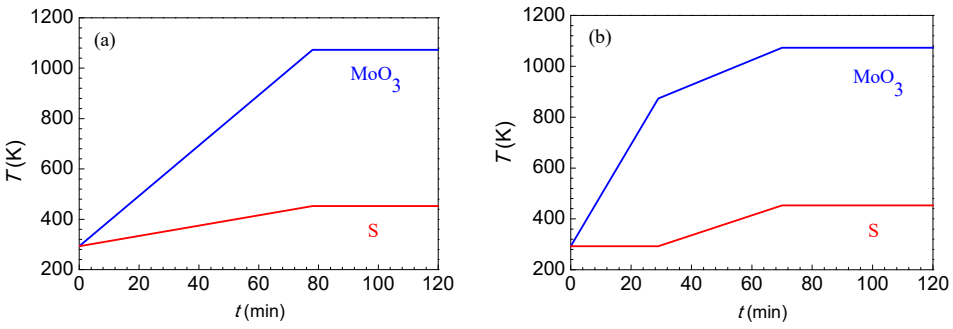

Figure 2. Heating methods to prepare MoS_2: (**a**) one-step heating and (**b**) two-step heating.

By using SEM to observe the surface morphology of the one-step heating sample, it was found that a large number of white particles or quadrilateral crystals (the intermediate product MoO_2) appeared on the surface of a large number of samples, as shown in Figure 3a.

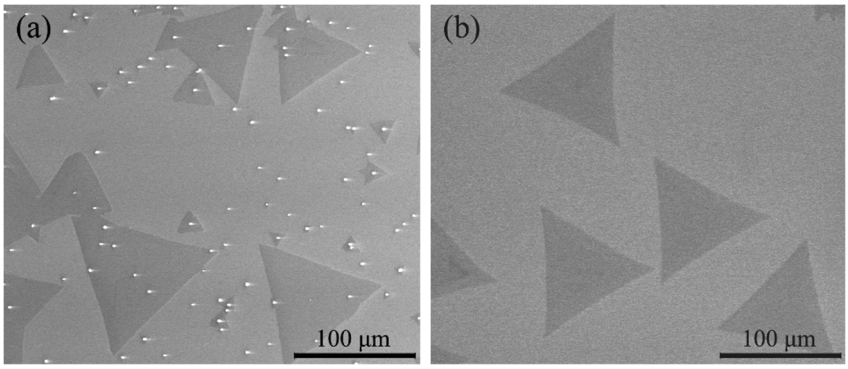

Figure 3. Scanning electron microscope (SEM) images of MoS_2 prepared by using the two heating methods: (**a**) one-step heating and (**b**) two-step heating.

The above experimental results can be explained in terms of the chemical reaction and phase transition of the Mo–S–O system. In the experimental temperature region, the following reactions and phase transition can occur in the Mo–S–O system:

$$2S_{(s)} \rightleftharpoons S_{2(g)} \quad (1)$$

$$S_{2(g)} + 2O_2 \rightleftharpoons 2SO_{2(g)} \quad (2)$$

$$MoO_{3(s)} \rightleftharpoons MoO_{3(g)} \ (T < 1068\ K) \quad (3)$$

$$MoO_{3(s)} \rightleftharpoons MoO_{3(l)} \ (T = 1068\ K) \quad (4)$$

$$MoO_{3(l)} \rightleftharpoons MoO_{3(g)} \ (T > 1068\ K) \quad (5)$$

$$MoO_{3(g)} + (x/2)S_{2(g)} \rightleftharpoons MoO_{3-x(g)} + (x/2)SO_2 \quad (6)$$

$$MoO_{3-x(g)} \rightleftharpoons MoO_{2(s)} + (1/2 - x/2)O_2 \quad (7)$$

$$MoO_{3-x(g)} + (7 - x)/S_{2(g)} \rightleftharpoons MoS_{2(g)} + (3 - x)/2SO_2 \quad (8)$$

$$MoS_{2(g)} \rightleftharpoons MoS_{2(s)} \quad (9)$$

The effect of temperature on a chemical reaction can be judged according to the dependence of its standard Gibbs free energy change (ΔG_0) on the temperature (T). If the dependence curve of ΔG_0 on T for a chemical reaction has a positive slope, as shown in Figure 4a, then the driving force of reaction decreases with rising temperature. On the contrary, the driving force of reaction increases with rising temperature when the slope of the curve is a negative, as shown in Figure 4b.

The slope of the dependence curve of ΔG_0 on T for a chemical reaction depends on the entropy change of the reaction (ΔS_0). When ΔS_0 is positive, the slope is negative. In contrast, the slope is positive if ΔS_0 is negative. It can be determined that the slopes of the dependence curve of ΔG_0 on T for the reactions of Equations (1), (3), and (5) are negative, which indicates that the driving force of the reaction increases with rising temperature, whereas the dependence curves of ΔG_0 on T for the reactions of Equations (2) and (7)–(9) are positive, which indicates that the driving force for the reaction decreases with rising temperature. Therefore, increasing temperature is favorable for the reactions of Equations (1), (3), and (5), but adverse for the reactions of Equations (2) and (7)–(9).

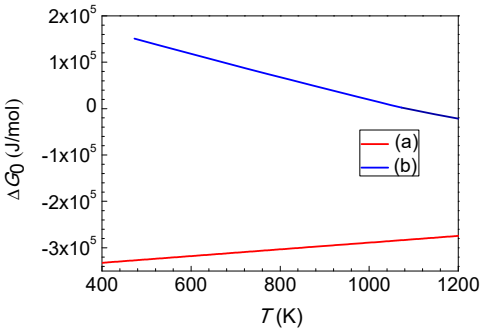

Figure 4. Dependence curve of the standard Gibbs free energy change (ΔG_0) on temperature (T) for the chemical reaction. (**a**) Positive slope ($\Delta S_0 < 0$); (**b**) negative slope ($\Delta S_0 > 0$).

The formation of MoO_2 depends on the reaction in Equation (7). The driving force of reaction for Equation (7) decreases with rising temperature. Therefore, the reaction of Equation (7) is easy to take place at low temperature. In addition, in one-step heating, S and MoO_3 sources are heated at the same time. The reaction of $S_{2(g)}$ and O_2 can decrease the concentration of O_2 in the furnace, which can promote the reaction of Equation (7) and produce $MoO_{2(s)}$. Therefore, if the heating of S and $MoO_{3(s)}$ starts at the same time, there are a large number of white or quadrilateral MoO_2 crystals, as shown in Figure 2a on the surface of the sample.

To reduce the formation of intermediate products, it is necessary to reduce the chance for $MoO_{3(g)}$ to contact with $S_{2(g)}$ at low temperatures. To achieve this purpose, a two-step heating method, as shown in Figure 2b, was employed. First, the MoO_3 zone was rapidly heated to 837 K at a rate of 20 K/min, and then slowly heated to 1098 K at a rate of 5 K/min. The heating of the S zone began at the time when the temperature of the MoO_3 zone was heated to 837 K, which can prevent the formation of MoO_2, since there is no chance for $MoO_{3(g)}$ and $S_{2(g)}$ to contact at a temperature lower than 837 K.

Figure 3b shows the morphology of the two-step heating sample. It can be seen that there are no MoO_2 white particles on the substrate, and the surface is very clean. In two-step heating, S has not yet sublimated when the temperature of MoO_3 is lower than 837 K, which avoids the contact of $MoO_{3(g)}$ and $S_{2(g)}$ at low temperatures and reduces the possibility of generating the intermediate product MoO_2.

3.2. Effect of Temperature on the Morphology and Layer Number of MoS_2 Crystals

The temperature directly affects the sublimation rate of MoO_3 and S, thus affecting the growth of MoS_2 crystal. To eliminate the influence of temperature on the volatilization rate and bring about a change in the S concentration in the tube furnace, the temperature of the low temperature zone is set at 453 K. The effect of the MoO_3 temperature (1048 K, 1073 K, 1098 K, 1123 K) on the growth of a single-layer MoS_2 crystal is studied with a molybdenum source dosage of 0.02 g, a holding time of 30 min, a gas flow rate of 100 sccm, and a distance between the carrier and the molybdenum source of 4~5.5 cm.

Figure 5 shows the effect of MoO_3 temperature on the morphology of a single-layer MoS_2 crystal obtained by SEM. It can be seen that, as shown in Figure 5a, there is almost nothing on the substrate when the temperature of MoO_3 is 1048 K. The reason for this is that at low temperatures, there is not enough MoO_3 sublimated, and the amount of MoO_3 participating in the chemical vapor deposition reaction is insufficient. When the temperature of MoO_3 is 1073 K, as shown in Figure 5b, the temperature in the high temperature zone just exceeds the melting point of MoO_3 (1068 K), which make it is possible for more MoO_3 to be evaporated and reduced by $S_{2(g)}$ to form MoS_2. The size of the single-layer MoS_2 depends on the evaporation pressure of MoO_3. As shown in Figure 6, the evaporation pressure of MoO_3 increases with rising temperature. When the temperature of MoO_3 is 1073 K, the side length of the triangular MoS_2 is approximately 30 μm. Obviously, the size of the triangular single-layer MoS_2 on the substrate is not sufficiently large. When the temperature of

MoO_3 is 1098 K, as shown in Figure 5c, an amount of complete and independent triangular MoS_2 crystals with a side length of approximately 100 μm appears. This results from the higher temperature increasing the evaporation rate of MoO_3 and the amount of MoO_3 evaporated, providing sufficient $MoO_{3(g)}$ to react with $S_{2(g)}$; thus, more MoS_2 is formed and deposited on the substrate for crystal growth. From Figure 5b,c, it can be seen that the grown single crystals are regular triangles, the surface colors of the single crystals are uniform, and the comparisons with the substrates are apparent. It can be preliminarily judged that the triangle crystals are single-layer.

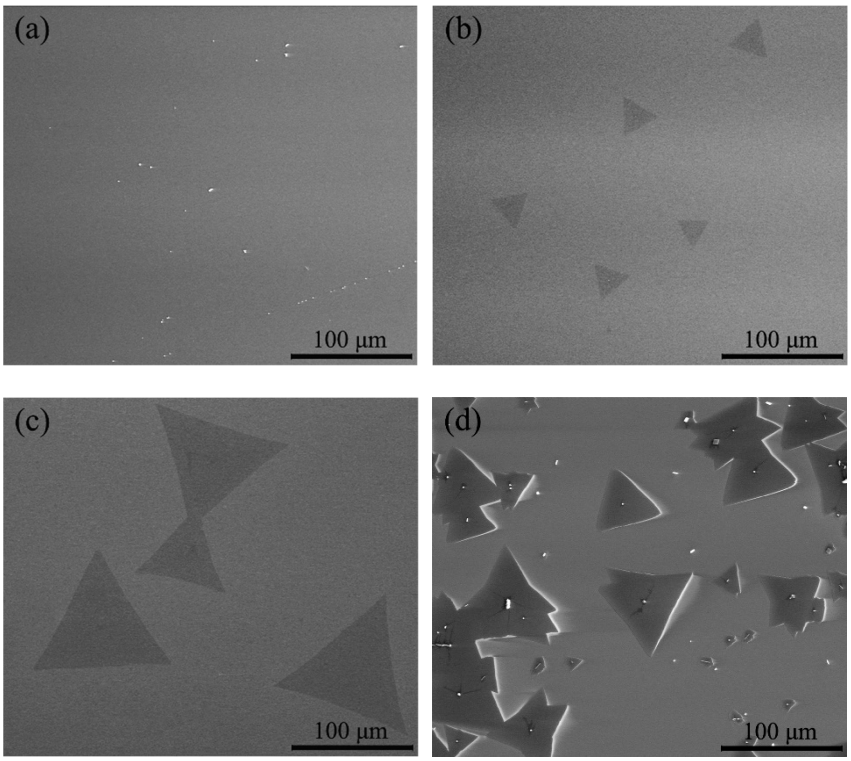

Figure 5. SEM images of MoS_2 prepared from different temperatures: (**a**) 1048 K, (**b**) 1073 K, (**c**) 1098 K, (**d**) 1123 K.

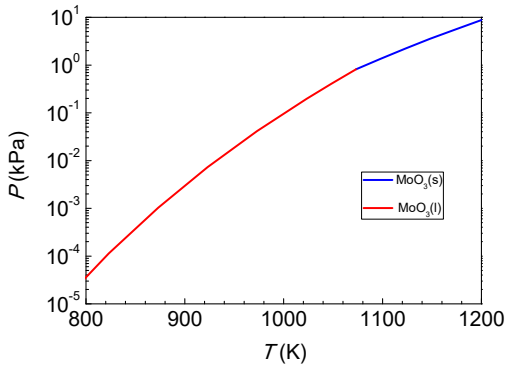

Figure 6. Dependence of the evaporation pressure P on the temperature T for MoO_3.

When the temperature of MoO_3 is 1123 K, as shown in Figure 5d, the size of MoS_2 does not become larger but diminishes. However, the MoS_2 crystal number increases under this condition: a large number of regular triangular MoS_2 crystals are contacted or stacked together to form multi-layered MoS_2. Since the ΔS_0 for Equation (5) is positive and ΔG_0 decreases with rising temperatures, the driving force of the reaction for Equation (5) increases with rising temperature. Therefore, when the temperature of MoO_3 rises to 1123 K, the evaporation pressure of MoO_3 is much higher, which can

increase the concentration of $MoS_{2(g)}$ in the furnace. The critical size of the atomic cluster for MoS_2 to form nucleation decreases with an increasing concentration of $MoS_{2(g)}$. The decrease of the critical size of the atomic cluster for MoS_2 to form nucleation can lead to the continuous formation of the MoS_2 crystal nucleus, thus suppressing its growth. Therefore, when the temperature of MoO_3 is 1123 K, a large number of multi-layered MoS_2 crystals are formed.

In addition, at this higher temperature, the evaporation rate of MoO_3 is much higher, and $MoO_{3(g)}$ cannot be completely reduced by $S_{2(g)}$ in time. The decomposition of the excessive $MoO_{3(g)}$ can form $MoO_{2(s)}$. Therefore, when the temperature of MoO_3 is 1123 K, the deposits on the substrate are a mixture of MoS_2 and disulfide.

3.3. Characterization of the MoS_2 Structure

3.3.1. Characterization by Raman Spectroscopy

Based on the Raman scattering effect, Raman spectroscopy can be used to study the structure of molecules by analyzing the scattering spectrum different from the incident light frequency. There are five vibration modes (E^2_{2g}, E^1_{2g}, E_{1g}, E_{1u}, and A_{1g}) in MoS_2. For the Raman spectroscopy test of MoS_2, only E^1_{2g} and A_{1g} modes are observed [22,23]. The characteristic peak position of the Raman spectrum of MoS_2 is related to the film thickness. The Van der Waals force increases as the layer number decreases. When the layer number of the film decreases gradually, the characteristic peak corresponding to the A_{1g} vibration mode happens to red shift (shifts to the long wavelength side), and the characteristic peak corresponding to the E^1_{2g} vibration mode happens to blue shift (shifts towards the blue end of the spectrum). When MoS_2 is a bulk material, the E^1_{2g} peak is located near 382 cm^{-1}, and the A_{1g} peak is located near 407 cm^{-1}. When the layer number of MoS_2 is reduced to a single layer, the E^1_{2g} peak shifts towards the blue end, to approximately 385 cm^{-1}, and the A_{1g} peak shifts to the long wavelength side, to approximately 403 cm^{-1}. The A_{1g} peak corresponding to MoS_2 film of different layers differs from the E^1_{2g} peak, and thus the layer number of MoS_2 could be determined based on the difference between the detected A_{1g} peak and E^1_{2g} peak [24]. Figure 7 shows the results of the clean sapphire substrate and the single-layer triangular MoS_2 samples deposited on the substrate obtained by Raman spectroscopy. By comparing Figure 7a,b, it can be inferred that the peak appearing at a wavenumber of 416 cm^{-1} in Figure 7b is caused by the influence of the sapphire substrate Al_2O_3. The temperature in the high temperature zone of sample 1 (the sample in Figure 5b) is 1073 K, and the temperature in the high temperature zone of the sample 2 (the sample in Figure 5c) is 1098 K. It can be seen that the E^1_{2g} peak of the single-layer triangular MoS_2 in the two samples is approximately 385 cm^{-1}, and the A_{1g} peak is approximately 403 cm^{-1}. The wavenumber difference is 19.2 cm^{-1} and 20.7 cm^{-1}, respectively. This indicates that the deposits on the sapphire substrate of sample 1 and sample 2 are single-layer MoS_2, which is consistent with the predicted results of SEM.

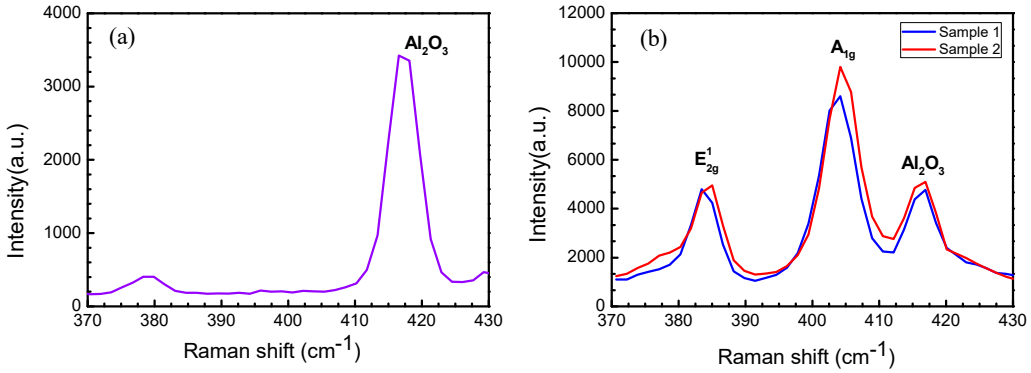

Figure 7. Raman spectra. (**a**) Clean sapphire substrate and (**b**) single-layer triangular MoS_2 samples deposited on the substrate. Sample 1: the temperature in the high temperature zone is 1073 K; Sample 2: the temperature in the high temperature zone is 1098 K.

3.3.2. Characterization of Photoluminescence Spectra

In bulk MoS_2, no photoluminescence is observed. When it is gradually thinned to a few layers, or even a single layer, the band gap of MoS_2 changes to a direct band gap, and the fluorescence effect is obviously enhanced, with two characteristic peaks appearing near 1.8 eV and 2.0 eV. The characteristic peak corresponding to 1.8 eV is the direct band gap of MoS_2, and the characteristic peak corresponding to 2.0 eV is the energy band splitting caused by the spin orbit coupling of MoS_2 [7,25]. The photoluminescence spectrum can be used as an effective means of characterizing the layer number of MoS_2. Figure 8 shows the results of the clean sapphire substrate and the single-layer triangular MoS_2 samples deposited on the substrate obtained by photoluminescence spectra. By comparing Figure 8a,b, it can be believed that the peak appearing at a wavelength of 692.7 nm in Figure 8b is caused by the influence of the sapphire substrate Al_2O_3. Sample 1 (the sample in Figure 5b) shows a strong characteristic peak at the wavelength of λ_1 = 665.8 nm, and sample 2 (the sample in Figure 5c) shows a strong characteristic peak at λ_2 = 671.4 nm. According to the Planck–Einstein relation, it can be determined that the corresponding transition energy level E = 1.86 eV at the luminescence peak λ_1 = 665.8 nm, and the corresponding transition energy level E = 1.85 eV at the luminescence peak λ_2 = 671.4 nm, which is in accordance with the band gap width of single layer MoS_2. It can be seen that both the characteristic peaks around 670 nm of two samples are intrinsic transition peaks, further verifying that the MoS_2 crystals deposited on the substrate in Figure 5b,c are of single-layer structures. By comparing the fluorescence efficiency of two samples at the characteristic peaks around 670 nm, it can be seen that the fluorescence efficiency of sample 1 is higher than that of sample 2.

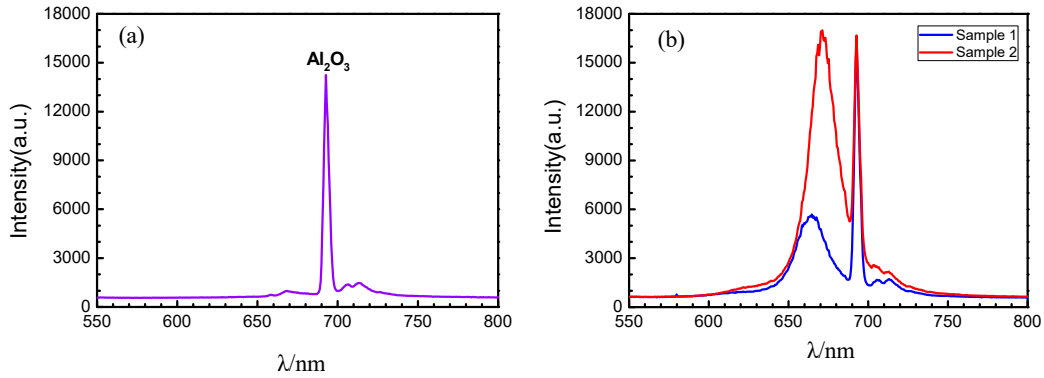

Figure 8. Photoluminescence spectra. (**a**) Clean sapphire substrate and (**b**) single-layer triangular MoS_2 samples deposited on the substrate. Sample 1: the temperature in the high temperature zone is 1073 K; Sample 2: the temperature in the high temperature zone is 1098 K.

4. Conclusions

(1) The two-step heating method to prepare MoS_2 is superior to the one-step heating method. Mixed compounds of MoO_2 and MoS_2 are easily formed by the one-step heating method. The two-step heating method can avoid the contact of $S_{2(g)}$ with $MoO_{3(g)}$ and the formation of MoO_2 at low temperatures.

(2) The growth of MoS_2 crystal depends on the temperature. Neither too low nor too high of a heating temperature of MoO_3 is conducive to the formation of MoS_2. In the range of 1073 K to 1098 K, the size of MoS_2 increases with the rise in temperature. A uniform large-sized triangle with a side length of 100 μm is obtained when the heating temperature of MoO_3 is 1098 K.

(3) The test results of SEM, Raman spectroscopy, and photoluminescence spectroscopy show that the triangular MoS_2 crystals grown by the two-step heating method are single-layer structures.

Author Contributions: H.C. and J.J. conceived and designed the experiments. J.J. and T.X. performed the synthesis experiments. J.J. and H.C. analyzed the data. J.J. and H.C. wrote the paper.

Funding: This work has been supported by the National Science Foundation of China (Grant Nos. 51575454 and 51671151).

Conflicts of Interest: The authors declare no conflict of interest.

References

1. Novoselov, K.S.; Geim, A.K.; Morozov, S.; Jiang, D.; Zhang, Y.; Dubonos, S.V.; Grigorieva, I.V.; Firsov, A.A. Discover of Graphene: Electric Field Effect in Atomically Thin Carbon Films. *Science* **2004**, *306*, 666–669. [CrossRef] [PubMed]
2. Novoselov, K.S.; Jiang, Z.M.; Zhang, Y.; Morozov, S.V.; Stormer, H.L.; Zeitler, U.; Maan, J.C.; Boebinger, G.S.; Kim, P.C.; Geim, A.K. Room Temperature Quantum Hall Effect in Graphene. *Science* **2007**, *315*, 1379. [CrossRef] [PubMed]
3. Mayorov, A.S.; Gorbachev, R.V.; Morozov, S.V.; Britnell, L.; Jalil, R.; Ponomarenko, L.A.; Blake, P.; Novoselov, K.S.; Watanabe, K.; Taniguchi, T.; et al. Micrometer-scale Ballistic Transport in Encapsulated Graphene at Room Temperature. *Nano Lett.* **2011**, *11*, 2396–2399. [CrossRef] [PubMed]
4. Wang, F.; Zhang, Y.B.; Tian, C.S.; Girit, C.; Zettl, A.; Crommie, M.; Shen, Y.R. Gate-variable optical transitions in Grapheme. *Science* **2008**, *320*, 206–209. [CrossRef] [PubMed]
5. Lu, Q.; Huang, R. Nonlinear Mechanics of Single-atomic-layer Graphene Sheets. *Int. J. Appl. Mech.* **2009**, *1*, 443–467. [CrossRef]
6. Mak, K.F.; Lee, C.; Hone, J.; Shan, J.; Heinz, T.F. Atomically Thin MoS_2: A New Direct Gap Semiconductor. *J. Phys. Rev. Lett.* **2010**, *105*, 136805. [CrossRef]
7. Splendiani, A.; Sun, L.; Zhang, Y.; Li, T.; Kim, J.; Chim, C.Y.; Galli, G.; Wang, F. Emerging Photoluminescence in Monolayer MoS_2. *Nano Lett.* **2010**, *10*, 1271–1275. [CrossRef]
8. Yoon, Y.; Ganapathi, K.; Salahuddin, S. How Good Can Monolayer MoS_2 Transistors Be? *Nano Lett.* **2011**, *11*, 3768–3773. [CrossRef]
9. Radenovic, A.; Brivio, J.; Giacometti, V.; Kis, A. Single-layer MoS_2 transistors. *Nat. Nanotechnol.* **2011**, *6*, 147–150.
10. De, S.; Kunal, K.; Aluru, N.R. Nonlinear Intrinsic Dissipation in Single Layer MoS_2 Resonators. *Rsc Adv.* **2017**, *7*, 6403–6410. [CrossRef]
11. Tang, H.J.; Wang, J.G.; Yin, H.J.; Zhao, H.J.; Wang, D.; Tang, Z.Y. Growth of Polypyrrole Ultrathin Films on MoS_2 Monolayers as High-Performance Supercapacitor Electrodes. *Adv. Mater.* **2015**, *27*, 1117–1123. [CrossRef] [PubMed]
12. Yin, Z.Y.; Li, H.; Li, H.; Jiang, L.; Shi, Y.M.; Sun, Y.H.; Lu, G.; Zhang, Q.; Chen, X.D.; Zhang, H. Single-layer MoS_2 Phototransistors. *Acs Nano* **2012**, *6*, 74–80. [CrossRef] [PubMed]
13. Lopez-Sanchez, O.; Lembke, D.; Kayci, M.; Radenovic, A.; Kis, A. Ultrasensitive photodetectors based on monolayer MoS_2. *Nat. Nanotechnol.* **2013**, *8*, 497. [CrossRef]
14. Wu, J.; Li, H.; Yin, Z.Y.; Li, H.; Liu, J.Q.; Cao, X.H.; Zhang, Q.; Zhang, H. Layer Thinning and Etching of Mechanically Exfoliated MoS_2 Nanosheets by Thermal Annealing in Air. *Small* **2013**, *9*, 3314–3319.
15. Zeng, Z.Y.; Sun, T.; Zhu, J.X.; Huang, X.; Yin, Z.Y.; Lu, G.; Fan, Z.X.; Yan, Q.Y.; Hng, H.H.; Zhang, H. An Effective Method for the Fabrication of Few-layer-thick Inorganic Nanosheets. *Angew. Chem. Int. Ed. Engl.* **2012**, *51*, 9052–9056. [CrossRef] [PubMed]
16. Ji, S.S.; Yang, Z.; Zhang, C.; Liu, Z.Y.; Weng, W.T.; Phang, I.Y.; Zhang, Z.; Pan, J.S.; Liu, T.X. Exfoliated MoS_2 Nanosheets as Efficient Catalysts for Electrochemical Hydrogen Evolution. *Electrochim. Acta* **2013**, *109*, 269–275. [CrossRef]
17. Lee, Y.H.; Zhang, X.Q.; Zhang, W.; Chang, M.T.; Lin, C.T. Synthesis of large-area MoS_2 atomic layers with chemical vapor deposition. *Adv. Mater.* **2012**, *24*, 2320–2325. [CrossRef] [PubMed]
18. Zhan, Y.J.; Liu, Z.; Najmaei, S.; Ajayan, P.M.; Lou, J. Large-area Vapor-phase Growth and Characterization of $MoS_{(2)}$ Atomic Layers on a $SiO_{(2)}$ Substrate. *Small* **2012**, *8*, 966–971. [CrossRef] [PubMed]
19. Li, W.; Birdwell, A.G.; Amani, M.; Burke, R.A.; Ling, X.; Lee, Y.H.; Liang, X.L.; Peng, L.M.; Richter, C.A.; Kong, J.; et al. Broadband Optical Properties of Large-area Monolayer CVD Molybdenumdisulfide. *Phys. Rev. B* **2014**, *90*, 195434. [CrossRef]
20. Zhang, W.; Huang, J.K.; Chen, C.H.; Chang, Y.H.; Cheng, Y.J.; Li, L.J. High-Gain Phototransistors Based on a CVD MoS_2 Monolayer. *Adv. Mater.* **2013**, *25*, 3456–3461. [CrossRef]

21. Lee, J.; Wang, Z.; He, K.; Shan, J.; Feng, P.X.L. High frequency MoS_2 nanomechanical resonators. *Acs Nano* **2013**, *7*, 6086–6091. [CrossRef]
22. Verble, J.L.; Wieting, T.J. Lattice Mode Degeneracy in MoS_2 and Other Layer Compounds. *Phys. Rev. Lett.* **1970**, *25*, 362–365. [CrossRef]
23. Verble, J.L.; Wieting, T.J.; Reed, P.R. Rigid-layer lattice vibrations and van der waals bonding in hexagonal MoS_2. *Solid State Commun.* **1972**, *11*, 941–944. [CrossRef]
24. Lee, C.; Yan, H.; Brus, L.E.; Heinz, T.F.; Hone, J.; Ryu, S. Anomalous lattice vibrations of single- and few-layer MoS_2. *Acs Nano* **2010**, *4*, 2695–2700. [CrossRef] [PubMed]
25. Mak, K.F.; He, K.L.; Shan, J.; Heinz, T.F. Control of valley polarization in monolayer MoS_2 by optical helicity. *Nat. Nanotechnol.* **2012**, *7*, 494–498. [CrossRef] [PubMed]